USE OF CFD METHODS FOR TRANSONIC WIND TUNNEL NOZZLE SELECTION

Nide G.C.R. Fico Jr.*, João L. F. Azevedo†, Marcos A. Ortega‡

Centro Técnico Aeroespacial
Instituto Tecnológico de Aeronáutica
12228-900 São José dos Campos - SP - BRAZIL

Abstract

A numerical investigation of the flowfield in three proposed geometries for the nozzle and contraction of a transonic wind tunnel facility is performed. The primary objective was to understand details of the flow in the tunnel in order to try to maximize test section flow quality. The calculations presented here include preliminary 2-D simulations and full 3-D computations. The codes used for the present calculations were previously validated by the authors and co-workers, and these validation studies are available in the literature. The primary flow solvers used implement an Euler formulation, and use the implicit approximate factorization Beam and Warming algorithm for the solution of the discretized equations. A boundary layer code was typically run at a post-processing stage in order to estimate boundary layer growth and its impact on flow quality. Results obtained for a sonic nozzle and for two Laval nozzles are presented, and they were instrumental in the selection process which led to the transonic facility which is currently being built.

Introduction

Transonic wind tunnels usually operate from low subsonic Mach numbers ($M \cong 0.25$) to the supersonic regime ($M \cong 1.6$). The tunnel nozzle is a key element in achieving the desired test-section Mach number, M_{TS}. Mach numbers up to unity are obtained using a sonic nozzle. There are two possible solutions for M_{TS} above this value: *(i)* the installation of a flexible Laval nozzle or *(ii)* a sonic nozzle used in conjunction with test-section mass extraction. In the case of test-section evacuation, about 2.5% of the tunnel total mass flow enters the plenum chamber through ventillated walls. While the first option is mechanically complex and much more expensive, it yields better test-section flow quality than the second one. Moreover, the second option is also limited to $M_{TS} \leq 1.3$, since above this test section Mach number value the mass extraction needed is prohibitive as it would demand very large auxiliary compressors and it would also have an adverse impact upon the tunnel flow quality.

Centro Técnico Aeroespacial (CTA) is designing a large transonic wind tunnel facility with a 2.0×2.4 m test section (TTS Project). To minimize the technical risks involved in such an enterprise, the project's first phase consists of the construction and operation of a Pilot facility (TTP). Among the many important points to be checked in the TTP emerges the nozzle design. The design of the nozzle is of utmost importance as it is directly related to the flow quality at the test section. On the other hand, Computational Fluid Dynamics (CFD) methods are enjoying increasing application assisting in the selection of tunnel airline component geometry[1]. These techniques have been used to design diffusers and flexible nozzles as well as investigate other aspects of the tunnel flow. Therefore, the major objective of the present work is to study, using CFD techniques, three possible nozzles for the TTP. One of them is a sonic nozzle, and the other two are Laval nozzles with a nominal Mach number of 1.3. It was decided that, in the TTP context, the optimum choice for the nozzle element would be to have fixed interchangeable nozzle blocks, instead of the flexible nozzle planned for the full size facility.

The calculations presented here include preliminary 2-D simulations and full 3-D computations. The codes used for the present calculations were previously validated by the authors and co-workers, and these validation studies are available in the literature[2]-[8]. Both for the 2-D and the 3-D case, an Euler formulation is implemented in the codes, and the Beam and Warming implicit approximate factorization algorithm[9]-[11] is used to discretize and solve the governing equations. The implicit Euler method is used for the time march and central differences are used to discretize the space derivatives. Artificial dissipation terms are explicitly added in order to control nonlinear instabilities. Considerable effort was invested in the accurate implementation of entrance and exit boundary conditions through the use of one-dimensional characteristic relations[6, 12]. The most stringent requirement for a tunnel nozzle, besides giving the desired test section Mach number, is the quality of the flow it provides for the test section. Therefore, the consideration of boundary layer growth is also an important issue in this case. Here, for the 3-D simulations, this is taken into account

* Associate Professor.
† Research Engineer and Visiting Professor.
‡ Professor.

by a viscous-inviscid coupling. A boundary layer formulation, solved in the direct mode, is implemented and coupled to the 3-D Euler solver previously described. The boundary layer code was typically run at a post-processing stage in order to estimate boundary layer growth and its impact on flow quality.

The present work will briefly describe the formulation of the codes used and it will concentrate on the discussion of the results for the nozzle geometries considered. We are particularly interested in evaluating whether the nozzles can indeed produced the desired test section Mach number and on the quality of the flow provided by the contraction to the test section. On the latter subject, the existence, or not, of any shocks produced by the nozzle wall, and the amount of boundary layer growth and flow skewness at the test section entrance are of primary interest.

Theoretical Formulation

The compressible Euler equations can be written in strong conservation-law form for general three dimensional, body-conforming, curvilinear coordinates[11] as

$$\frac{\partial \overline{Q}}{\partial \tau} + \frac{\partial \overline{E}}{\partial \xi} + \frac{\partial \overline{F}}{\partial \eta} + \frac{\partial \overline{G}}{\partial \zeta} = 0 \tag{1}$$

where the vector of conserved quantities, $\overline{Q}$, is defined as

$$\overline{Q} = J^{-1} \begin{Bmatrix} \rho \\ \rho u \\ \rho v \\ \rho w \\ e \end{Bmatrix} \tag{2}$$

The flux vectors $\overline{E}$, $\overline{F}$ and $\overline{G}$ can be written as

$$\overline{E} = J^{-1} \begin{Bmatrix} \rho U \\ \rho u U + p\xi_x \\ \rho v U + p\xi_y \\ \rho w U + p\xi_z \\ (e+p)\,U - p\xi_t \end{Bmatrix} \tag{3}$$

$$\overline{F} = J^{-1} \begin{Bmatrix} \rho V \\ \rho u V + p\eta_x \\ \rho v V + p\eta_y \\ \rho w V + p\eta_z \\ (e+p)\,V - p\eta_t \end{Bmatrix} \tag{4}$$

$$\overline{G} = J^{-1} \begin{Bmatrix} \rho W \\ \rho u W + p\zeta_x \\ \rho v W + p\zeta_y \\ \rho w W + p\zeta_z \\ (e+p)\,W - p\zeta_t \end{Bmatrix} \tag{5}$$

In the above equations, the usual nomenclature is being used. Therefore, ρ is the density, u, v and w are the cartesian components of velocity, and e is the total energy per unit of volume. The equations have been nondimensionalized following the work of Azevedo[3]. Hence, density is made dimensionless with respect to the stagnation density at the nozzle entrance conditions, ρ_t, and velocity components are referred to the critical speed of sound at the nozzle entrance conditions, a_*. Pressure and total energy per unit of volume are referred to $\rho_t a_*^2$ and the specific internal energy is nondimensionalized with respect to a_*^2.

The pressure, p, can be obtained by the equation of state for perfect gases

$$p = (\gamma - 1)\,\rho e_i = (\gamma - 1)\left[e - \frac{1}{2}\rho\left(u^2 + v^2 + w^2\right)\right] \tag{6}$$

where e_i is the specific internal energy of the fluid, and γ is the ratio of specific heats. The contravariant velocity components are defined as

$$\begin{aligned} U &= \xi_t + \xi_x u + \xi_y v + \xi_z w \\ V &= \eta_t + \eta_x u + \eta_y v + \eta_z w \\ W &= \zeta_t + \zeta_x u + \zeta_y v + \zeta_z w \end{aligned} \tag{7}$$

Throughout this work, the Cartesian coordinate system is defined such that x is the direction along the axis of the tunnel, positive from upstream to downstream, and the y- and z-directions form a right-handed system with z positive upwards. The curvilinear coordinate system is defined such that ξ is the longitudinal direction, η is the nominally wall-normal direction which spans the tunnel from the centerline to the wall, and ζ is the circumferential direction. This coordinate system is obtained from the transformation of variables

$$\begin{aligned} \tau &= t \\ \xi &= \xi(x, y, z, t) \\ \eta &= \eta(x, y, z, t) \\ \zeta &= \zeta(x, y, z, t) \end{aligned} \tag{8}$$

The Jacobian of the transformation, J, can be expressed as

$$\begin{aligned} J = &\left(x_\xi y_\eta z_\zeta + x_\eta y_\zeta z_\xi + x_\zeta y_\xi z_\eta \right. \\ &\left. - x_\xi y_\zeta z_\eta - x_\eta y_\xi z_\zeta - x_\zeta y_\eta z_\xi\right)^{-1} \end{aligned} \tag{9}$$

Expressions for the various metric relations can be found, among other references, in Pulliam and Steger[11, 13].

The 2-D formulation is a straightforward simplification of the previously given equations in which one of the coordinate directions is considered infinite. We have considered the geometry of the tunnel vertical plane that passes through the tunnel centerline for the present 2-D simulations. More details of the 2-D formulation can be seen, for instance, in Refs. [3], [5], and [6]. The effective flow displacement due to viscous effects close to solid walls was predicted by a boundary layer code developed by Rotta[14]. This is a direct-type, integral method, with the following main capabilities: (*i*) prediction of laminar and/or turbulent boundary layers;

(*ii*) two laminar-turbulent transition criteria; (*iii*) appropriate treatment of shock wave interaction with the boundary layer.

Numerical Implementation

The previously given governing equations were implemented through the use of finite difference methods. The implicit Euler method was used for the time-march, and the spatial derivatives were approximated by three-point, second order central differences. The Beam and Warming implicit approximate factorization scheme[9, 10] was used for the solution of the resulting finite difference equations in order to obtain a cost efficient algorithm. The resulting scheme is second order accurate in space, as mentioned, but it is only first order accurate in time due to the use of the implicit Euler method.

The factored finite difference equations can be written in the delta form as[2]

$$L_\eta L_\zeta L_\xi \Delta_t \overline{Q}^n = R_\xi + R_\eta + R_\zeta \qquad (10)$$

The various operators are defined as

$$\begin{aligned}
L_\xi &= \left(I + \Delta t \delta_\xi \hat{A}^n - \epsilon_I \Delta t J^{-1} \nabla_\xi \Delta_\xi J\right) \\
L_\eta &= \left(I + \Delta t \delta_\eta \hat{B}^n - \epsilon_I \Delta t J^{-1} \nabla_\eta \Delta_\eta J\right) \\
L_\zeta &= \left(I + \Delta t \delta_\zeta \hat{C}^n - \epsilon_I \Delta t J^{-1} \nabla_\zeta \Delta_\zeta J\right) \\
R_\xi &= -\Delta t \delta_\xi \overline{E}^n - \epsilon_E \Delta t J^{-1} \left(\nabla_\xi \Delta_\xi\right)^2 J \overline{Q}^n \qquad (11) \\
R_\eta &= -\Delta t \delta_\eta \overline{F}^n - \epsilon_E \Delta t J^{-1} \left(\nabla_\eta \Delta_\eta\right)^2 J \overline{Q}^n \\
R_\zeta &= -\Delta t \delta_\zeta \overline{G}^n - \epsilon_E \Delta t J^{-1} \left(\nabla_\zeta \Delta_\zeta\right)^2 J \overline{Q}^n
\end{aligned}$$

In the above, δ_ξ, δ_η and δ_ζ are central difference operators; ∇_ξ, ∇_η and ∇_ζ are backward difference operators; and Δ_ξ, Δ_η and Δ_ζ are forward difference operators in the ξ- , η- and ζ-directions, respectively. As an example,

$$\begin{aligned}
\delta_\xi \overline{Q}^n_{i,j,k} &= \frac{1}{2}\left[\overline{Q}^n_{i+1,j,k} - \overline{Q}^n_{i-1,j,k}\right] \\
\nabla_\xi \overline{Q}^n_{i,j,k} &= \overline{Q}^n_{i,j,k} - \overline{Q}^n_{i-1,j,k} \qquad (12) \\
\Delta_\xi \overline{Q}^n_{i,j,k} &= \overline{Q}^n_{i+1,j,k} - \overline{Q}^n_{i,j,k}
\end{aligned}$$

The Δ_t is a forward difference operator in time given by

$$\Delta_t \overline{Q}^n = \overline{Q}^{n+1} - \overline{Q}^n \qquad (13)$$

Artificial dissipation terms have been introduced in the operators described by Eq. 11 in order to maintain the stability of the numerical solution process. Fourth order numerical dissipation terms were added to the right-hand side operators, and second order terms were used in the left-hand side operators. From an accuracy standpoint, one would like to also use fourth order artificial dissipation in the implicit operators. However, computational efficiency constraints prevent such use. The flux Jacobian matrices $\hat{A}^n$, $\hat{B}^n$ and $\hat{C}^n$ are described in detail elsewhere in the literature (see, for instance, Pulliam and Steger[13]).

Boundary Conditions

The three-dimensional simulations here presented take advantage of the double geometric symmetry existing in the nozzles considered in order to reduce the computational effort. Hence, only one-quarter of the complete nozzles are represented, and flow symmetry boundary conditions are enforced at both the vertical and horizontal symmetry planes. This is clearly assuming that flow conditions at the entrance of the computational domain are symmetric or, in other words, that the flow velocity at the entrance of the contraction is aligned with the tunnel axis. Such an assumption does represent a simplification in the sense that some misalignment can certainly occur, especially for closed circuit tunnels. In the present case, we have decided to neglect this effect mainly due computational power limitations and because the TTP is not a closed circuit facility. The symmetry boundary conditions are computationally enforced by allowing for an extra plane of grid points on the other side of the symmetry plane and forcing the appropriate symmetry, or anti-symmetry, of the conserved variables. Hence, boundary conditions in the ζ-direction are always symmetry, or reflection, conditions in the present case.

Due to the present code data structure, it is very difficult to strongly impose the flow tangency condition at the wall, at least at the boundary condition enforcement stage. Hence, the wall boundary condition is implemented by extrapolating all conserved variables from the computational surface adjacent to the wall, when explicitly enforcing the boundary conditions, and by imposing a zero convective flux in the wall normal direction in the residue computation. The reader should observe that, with such an scheme, the residue calculation sees the exact wall boundary condition at every time step, whereas the value of the conserved variables at the wall is progressively improved, as convergence is advanced, in order to reflect the correct flow tangency condition. Nozzle axis boundary condition is also implemented by extrapolating and by imposing a no-flux condition across the axis. A further complication arises in this case because the axis is a singularity of the transformation, in the sense that a line in physical space corresponds to a full plane in computational space. Hence, properties at a given point along the axis are obtained by extrapolating from the adjacent point (in the η-direction) and, then, averaging all values in the ζ-direction. The residue calculation is also modified in the centerline case in order to enforce the no-flux condition across the centerline.

Nozzle entrance and exit conditions are enforced using the concept of one-dimensional characteristic relations for the Euler equations. The concept is described

in the 2-D case by MacCormack[15]. Complete details for its implementation in two dimensions for both the planar and the axisymmetric case are described in Ref. [6]. The present three-dimensional computations have used these ideas in order to define how many quantities should be specified at each boundary and how many should be extrapolated from interior information. However, in order to simplify the implementation, the actual extrapolation process (of whatever quantities should be extrapolated) does use the characteristic relations but simple zero-th order extrapolation. As the authors have done in previous work[6], the stagnation pressure, the stagnation temperature and the flow entrance angle are specified at a subsonic entrance. The exit static pressure is fixed at a subsonic exit and, as determined by a characteristic relation analysis, no property can be specified at a supersonic exit. Aside from the fact that zero-th order extrapolation is being used for the actual extrapolation process, the treatment of entrance and exit conditions here is an exact extension to 3-D of the ideas discussed in Refs. [3] and [6], and the interested reader is referred to these references for further details.

All boundary conditions in the two-dimensional simulations were treated precisely as presented in Refs. [3] and [6], and they will not be further discussed here.

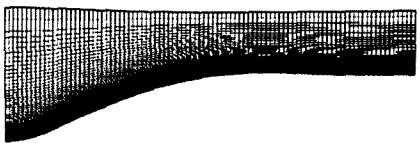

Figure 1: View of a typical 2-D computational grid

Results and Discussion

Initial evaluation of the proposed nozzles was performed using a two-dimensional formulation. It is clear that the flowfield in the nozzles considered in the present work is truly 3-D. However, these initial 2-D calculations already pointed out some of the difficulties associated with obtaining high test section flow quality. A typical grid used for the 2-D simulations is presented in Fig. 1. This particular configuration corresponds to one of the proposed Laval nozzles, and the grid shown has 94 × 59 grid points. The 2-D grids were generated by algebraic methods and exponential grid stretching functions were used in order to cluster grid points towards the nozzle wall, in the η-direction, and towards the throat, in the ξ-direction. The wall contours for all three nozzles treated in the present 2-D simulations are shown in Figs. 2 and 3.

As an example of the type of results which can be obtained with the 2-D calculations, Figs. 4 and 5 present wall pressure distributions along the two Laval nozzles axis for a nominal test section Mach number of 1.3. It is clear from these figures that the much gentler expansion associated with geometry *a* yields compression waves that are weaker than those generated by geometry *b*. Compression waves at the nozzle should be avoided because they introduce undesirable disturbances at the test section. According to the results shown in Figs. 4 and 5, geometry *a* is a better nozzle candidate than geometry *b* for the $M_{TS} = 1.3$ case. Wall pressure distributions for the sonic nozzle

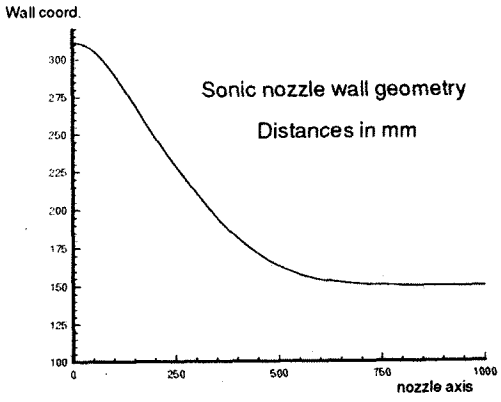

Figure 2: 2-D wall geometry for the sonic nozzle

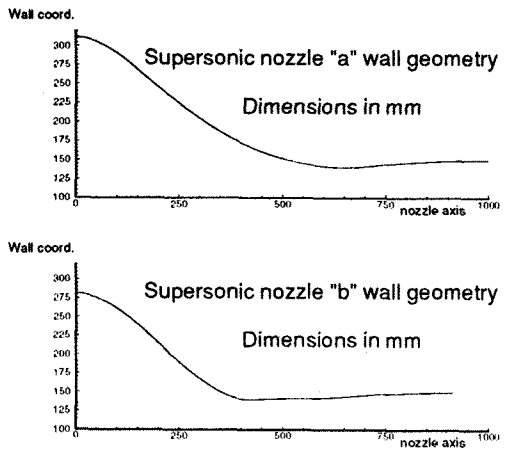

Figure 3: 2-D wall geometry for the Laval nozzles.

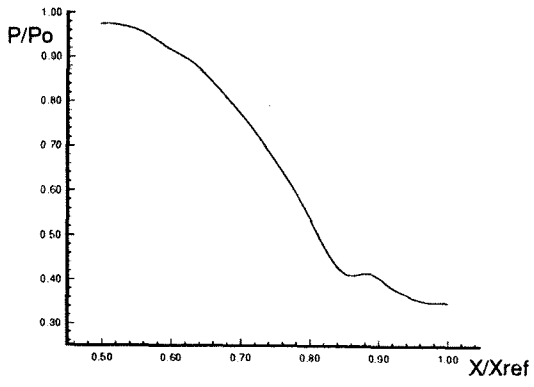

Figure 4: Wall pressure distribution in the streamwise direction for geometry a, nominal $M_{TS} = 1.3$ (2-D simulation).

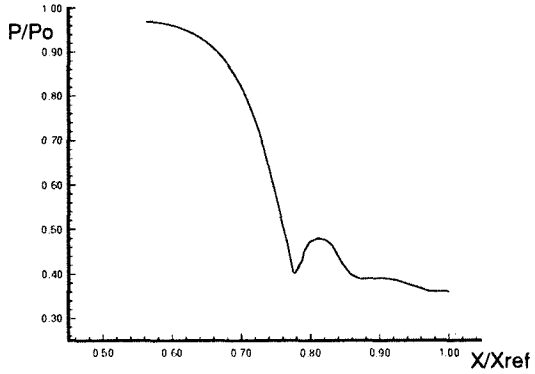

Figure 5: Wall pressure distribution in the streamwise direction for geometry b, nominal $M_{TS} = 1.3$ (2-D simulation).

are shown in Fig. 6 for a nominal test section Mach number of 0.6.

The 3-D calculations were performed using a 100 × 20 × 29 mesh points. Fig. 7 shows an overall view of a typical computational grid used in this work. The 3-D grids were also generated by algebraic methods, after the wall surface definition was provided by a CAD system. Particular attention was dedicated to obtain a detailed definition of the transition from the circular entrance section to the quadrilateral geometry of the throat and downstream regions. It should be noted that we have taken advantage of the nozzle double symmetry in order to reduce computational costs.

The Mach number contours at planes perpendicular to the streamwise direction are shown in Figs. 8 and 9, for geometries a and b, respectvely. These four planes correspond to $i = 1$ (entrance plane), two interior planes $i = 25$ and 75 and $i = 100$ (exit plane). The misleading impression of a very non-uniform behaviour rapidly disappears as one takes a close look at the values shown by the graphic scales. In fact, both Laval nozzles have a very smooth Mach number distribution at planes along their longitudional axis. Geometry a has the further advantage of producing at its exit plane a very uniform flow at the nozzle nominal Mach number of 1.3.

Other relevant results are plotted in Figs. 10 and 11. They show Mach number contours at the nozzle symmetry planes for geometry a and geometry b, respectively. The upper portion of both figures represent the plane $\theta = 90$ deg, while at the lower part the Mach number contours for the plane $theta = 0$ deg appear. Contrary

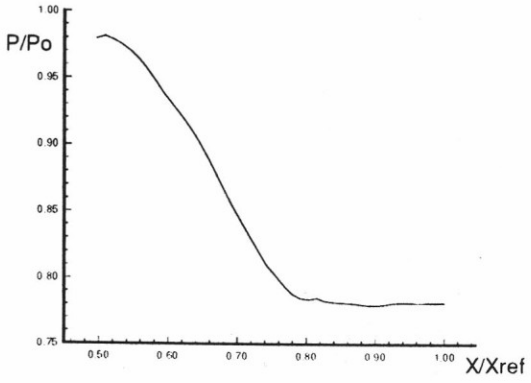

Figure 6: Wall pressure distribution in the streamwise direction for the sonic nozzle, nominal $M_{TS} = 0.6$ (2-D simulation).

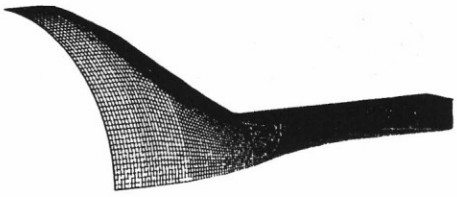

Figure 7: View of a typical 3-D computational grid.

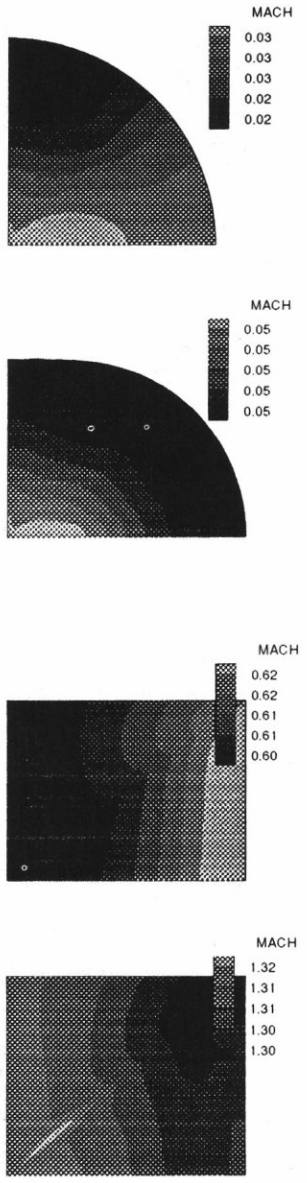

Figure 8: Mach number countours at planes perpendicular to the nozzle axis for geometry *a*, nominal $M_{TS} = 1.3$.

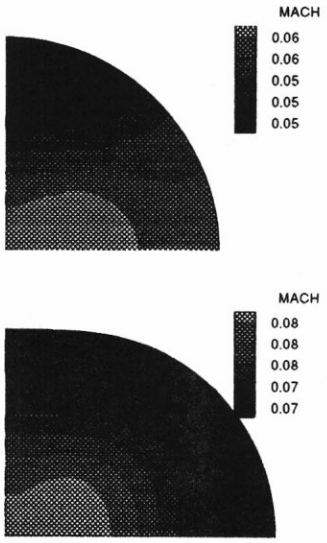

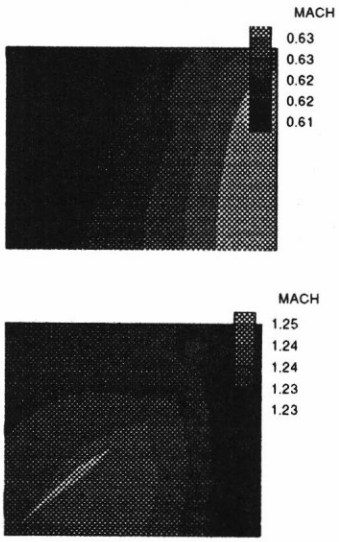

Figure 9: Mach number countours at planes perpendicular to the nozzle axis for geometry *b*, nominal $M_{TS} = 1.3$.

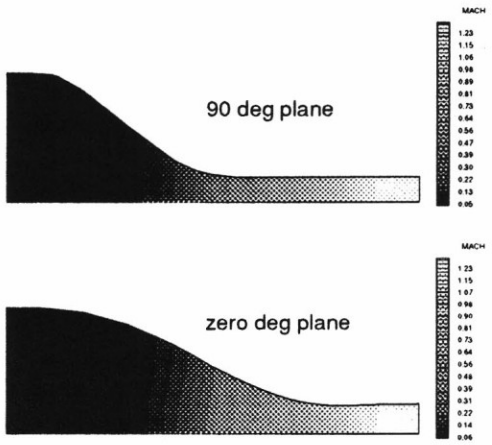

Figure 10: Mach number contours at the symmetry planes for geometry *a*.

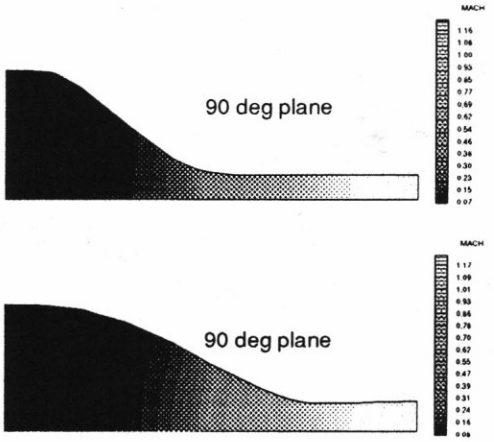

Figure 11: Mach number contours at the symmetry planes for geometry *b*.

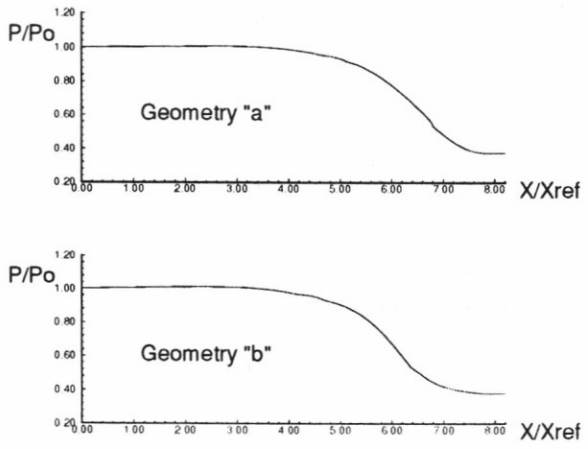

Figure 12: Pressure distribution in the streamwise direction for geometry a (upper one) and for geometry b (lower one) (3-D simulation).

to the 2-D results (see figures 4 and 5 in which shock waves appeared in both geometries, the 3-D solution points to a gentle expansion. The Mach lines in both cases are now fairly straight and extend themselves in the radial direction. It appears that the presence of the side walls, not accounted for in the 2-D case, helps guiding the flow more smoothly throught the nozzle. Moreover, the 90 deg-plane pressure distributions along both nozzles, shown in Fig. 12, present a monotonic behavior, unlike the 2-D results. This is highly desirable as shock waves have a tendency to "bump around" introducing flow disturbances at the test section.

The sonic nozzle is responsible for feeding the test section with flow with Mach numbers up to 1.2. As usual in wind tunnel operation, low supersonic speeds are obtained with sonic nozzles plus test section mass extraction [16]. As an example of the flow quality that might be expected from the sonic nozzle simulated here, Figs. 13 and 14 are presented. These results demonstrate that a very uniform flow is produced along the entire nozzle length. If one observes the lower plot in Fig. 14, which represents the nozzle exit plane, it is clear that the test section is being supplied with a very high quality flow.

The pressure distributions for the Laval nozzles obtained through the solution of the 3-D Euler equations were used as input for the boundary-layer solver[14]. The results appearing in Table 1 are for the symmetry planes ($\theta = 0$ and 90 deg) and for the plane $\theta = 45$ deg. Geometry a shows a smaller value of the boundary-layer thickness, δ, at the the nozzle exit than geometry

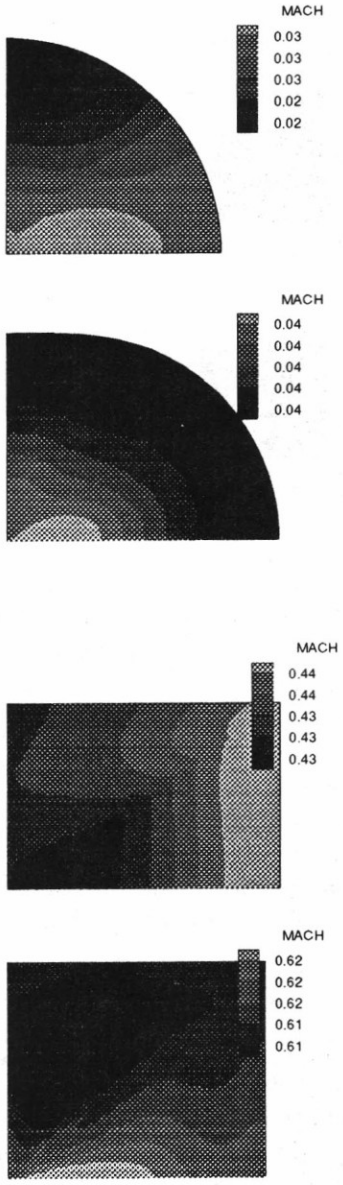

Figure 13: Mach number countours at planes perpendicular to the nozzle axis for the sonic nozzle, nominal $M_{TS} = 0.6$.

Table 1: Boundary-layer thickness at the exit plane for both Laval nozzles .

θ plane	$\delta(mm)$	
	Geom a	Geom b
0	4.66	5.84
45	4.65	5.67
90	4.52	5.43

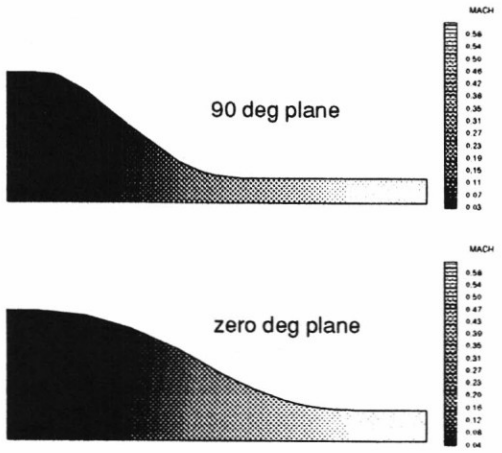

Figure 14: Mach number contours at the nozzle symmetry planes, nominal $M_{TS} = 0.6$.

b. Further, its azimutal variation of δ is smaller. These two aspects are important when one remembers that the test-section walls must be diverged by a small angle to compensate for boundary-layer growth. The results indicate that geometry *a* demands less and more uniform wall divergence and, therefore, proves once more to be superior than geometry *b* as a nozzle candidate.

Concluding Remarks

In summary, the present work has used CFD techniques to performed 2-D and 3-D simulations of transonic wind tunnel nozzles. The flow was modeled with the aid of the Euler equations. In order to study the main viscous effects, in particular boundary-layer thickness at the test section entrance, the 3-D results were, then, used as input to a boundary-layer solver[14]. The full 3-D calculations seem to corroborate the earlier 2-D results in the sense that they point to geometry *a* as being a better nozzle candidate. The sonic nozzle studied proved to be able to give high-quality test section flow. These simulations are being used in an actual design environment in order to aid in the selection of appropriate nozzle geometries to equip the TTP facility which is currently being constructed.

Acknowledgments

The present work was partially supported by Conselho Nacional de Desenvolvimento Científico e Tecnológico, CNPq, under grant number 530109/93-0.

References

1. Davis, M.W., Gunn, J.A., Herron, R.D., and Kraft E.M., "Optimum Transonic Wind Tunnel", AIAA 14th Aerodynamic Testing Conference, West Palm Beach, Florida, March 5-7, 1986.

2. Azevedo, J.L.F., "Aerodynamic Flow Simulation Using a Finite Difference Method," *Proceedings of the 2nd National Meeting of the Thermal Sciences*, Águas de Lindóia, SP, Brazil, Dec. 1988, pp. 3-6.

3. Azevedo, J.L.F., "Euler Solutions of Transonic Nozzle Flows," *Proceedings of the 3rd Brazilian Thermal Science Meeting*, Vol. I, Itapema, SC, Brazil, Dec. 1990, pp. 243-248.

4. Azevedo, J.L.F., Zdravistch, F., and Silva, A.F.C., "Implementation and Validation of Euler Solvers for Launch Vehicle Flows," *Proceedings of the 4th International Symposium on Computational Fluid Dynamics*, Vol. I, Davis, CA, Sept. 1991, pp. 42-47.

5. Ortega, M.A., and Azevedo, J.L.F., "Checking the Influence of Longitudinal Wall Curvature in the Implementation of Boundary Conditions at the Wall of a Convergent-Divergent Nozzle," *Proceedings of the 11th Brazilian Congress of Mechanical Engineering*, São Paulo, SP, Dec. 1991.

6. Azevedo, J. L. F., Fico Jr., N. G. C. R., Ortega, M. A., and Luna G. C., "Nozzle Flow Calculations Using the Euler Equations," ICAS Paper 92-4.1.2, *Proceedings of the 18th Congress of the International Council of Aeronautical Sciences*, Vol. 1, Beijing, China, Sept. 1992, pp. 97-107.

7. Azevedo, J.L.F., "A Finite Difference Method Applied to Internal Axisymmetric Flows," Panamerican Workshop for Applied and Computational Mathematics, Caracas, Venezuela, Jan. 1993.

8. Azevedo, J.L.F., Moraes, P., Jr., Maliska, C.R., Marchi, C.H., and Silva, A.F.C., "Code Validation for High Speed Flow Simulation over the VLS Launcher Fairing," AIAA Paper 93-3046, AIAA 24th Fluid Dynamics Conference, Orlando, FL, July 1993.

9. Beam, R.M., and Warming, R.F., "An Implicit Finite-Difference Algorithm for Hyperbolic Systems in Conservation-Law Form," *Journal of Computational Physics*, Vol. 22, 1976, pp. 87-110.

10. Beam, R.M., and Warming, R.F., "An Implicit Factored Scheme for the Compressible Navier-Stokes Equations," *AIAA Journal*, Vol. 16, No. 4, April 1978, pp. 393-402.

11. Pulliam, T.H., and Steger, J.L., "Implicit Finite-Difference Simulations of Three-Dimensional Compressible Flow," *AIAA Journal*, Vol. 18, No. 2, Feb. 1980, pp. 159-167.

12. Fico, N.G.C.R., Jr., "Simulation of the Flow in the Reentry Flap Region. of a Transonic Wind Tunnel," Doctoral Dissertation, Instituto Tecnológico de Aeronáutica, São José dos Campos, SP, Brazil, Jul. 1991.

13. Pulliam, T.H., and Steger, J.L., "Recent Improvements in Efficiency, Accuracy and Convergence for Implicit Approximate Factorization Algorithms," AIAA Paper 85-0360, AIAA 23rd Aerospace Sciences Meeting, Reno, Nevada, Jan. 1985.

14. Rotta, J.C., "Fortran IV - Rechenprogram für Grenzschichten bei Kompressiblen Ebenen und Achsensymmetrischen Strömungen," DLR-FB 71-51, DFVLR-AVA, Institut für Strömungsmechanik, Göttingen, 1971.

15. MacCormack, R.W., "An Introduction and Review of the Basics of Computational Fluid Dynamics," AIAA Professional Study Series on Computational Fluid Dynamics, Snowmass, Colorado, June 1984.

16. Goethert, B.H., "Transonic Wind Tunnel Testing," Pergamon Press, New York, 1961.